

## Conformational Analyses and MO Studies of f152A1 and Its Analogues as Potent Protein Kinase Inhibitors

Megumi Ikemori-Kawada,<sup>†</sup> Takatoshi Kawai,<sup>†</sup> Masaki Goto,<sup>†</sup> Yuan John Wang,<sup>‡</sup> and Yoshiyuki Kawakami<sup>\*,†</sup>

Eisai Tsukuba Research Laboratories, 1-3, Tokodai 5-chome, Tsukuba-shi, Ibaraki 300-2635, Japan, and Eisai Research Institute of Boston, 4 Corporate Drive, Andover, Massachusetts 01810

Received August 19, 2009

f152A1 was isolated from a fermentation broth of *Curvularia verruculosa* and characterized as a potent inhibitor of TNF $\alpha$  transcription, with anti-inflammatory activity. f152A1 and several analogues displayed inhibitory activity against the MAP kinases ERK2 and MEK1 in *in vitro* kinase assays. Through SAR studies on f152A1 and analogues prepared via total synthesis, we have identified structural features that contribute to inhibitory activity. To rationalize these results and to aid in the discovery process, a combination of high temperature molecular dynamics and MOPAC AM1 semiempirical molecular orbital method studies was used in studies that yielded a postulated active conformation, M1(8). This active conformation M1(8) reflects a high degree of conformational similarity among f152A1 and its more potent analogues. In view of the highly reactive *cis*-enone moiety in the flexible 14-membered resorcylic acid lactone ring of f152A1, the chemical reactivities of the enone moieties in various analogues were assessed by molecular orbital calculations. The enone reactivity analyses suggested that these inhibitors were prone to Michael addition at the  $\alpha,\beta$ -unsaturated ketone moiety and might chemically react with cysteine residues in the ATP-binding site of MAP kinases. Reactivity of the *cis*-enone moiety and the M1(8) conformation make important contributions to the inhibitory activity of MAP kinases.

### INTRODUCTION

During the course of screening for the inhibitors of TNF $\alpha$  transcription, f152A1 (Figure 1), (3S,5Z,8S,9S,11E)-8,9,16-trihydroxy-14-methoxy-3-methyl-3,4,9,10-tetrahydro-1*H*-2-benzoxacyclotetradecine-1,7(8*H*)-dione, isolated from the fermentation broth of a fungus, *Curvularia verruculosa*, was found by us to be a potent inhibitor of TNF $\alpha$  transcription.

This compound was originally discovered and reported as LL-Z1640-2,<sup>1</sup> and later described as 5Z-7-oxo-zeaenol<sup>2</sup> or as FR148083.<sup>3</sup> FR148083 was recently reported to inhibit ERK2 enzyme activity and TGF $\beta$ -induced AP-1-dependent luciferase expression.<sup>4,5</sup> In addition, an X-ray crystal structure of the ERK2/FR148083 complex and structure–activity relationships (SAR) suggested that both the *cis*-enone and the conformation of the 14-membered resorcylic acid lactone ring contribute to this inhibitory activity. This structure revealed that the compound binds to the ATP binding site of ERK2, involving a covalent bond to Sy of ERK2 Cys166. The authors concluded that covalent binding to the common cysteine residue in the ATP-binding site is likely to play a crucial role in the inhibitory activity against MAP kinases. Consistent with these findings, it has also been reported that hypothemycin<sup>6,7</sup> inhibits a subset of  $\sim$ 45 known Ser/Thr/Tyr protein kinases containing a cysteine residue corresponding to Cys166 of ERK2.<sup>8</sup> In addition, recent molecular modeling studies and the crystal structure of an ERK2–hypo-

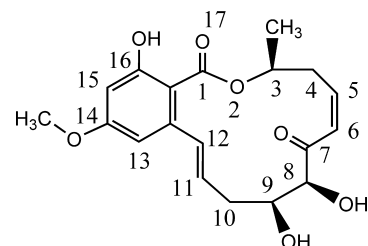


**Figure 1.** Molecular structure of f152A1 (**1**).

emycin complex suggest that hypothemycin forms a similar complex in which the Sy of the cysteine approaches hypothemycin from the *re*-face of the double bond, and a covalent adduct with *R*-stereochemistry is formed.<sup>9</sup>

As reported by Goto et al.,<sup>10,11</sup> we previously showed that the 5,6-enone reduced form of f152A1, **4**, had much reduced inhibitory activity against TNF $\alpha$  transcription ( $IC_{50}$  value  $>10\,000$ ; Table 1). The 11,12-epoxy derivative, **2**, largely retained activity, but the *trans*-enone analogue, **3**, showed reduced activity, with an  $IC_{50}$  value approximately 32-fold greater than that of f152A1. These SAR studies with **1** and synthetic versions of the naturally occurring analogues **2**, **3**, and **4** suggested that both the  $\alpha,\beta$ -unsaturated enone and the conformation of the lactone ring contribute to inhibitory activity.

The *in silico* SAR studies presented here were used to investigate structural contributions to inhibitory activity as a function of modification in the f152A1 class of inhibitors. The studies included conformational search and reactivity analysis using a combination of high temperature molecular dynamics (HTMD)<sup>12</sup> and MOPAC AM1<sup>13</sup> semiempirical molecular orbital calculations.

\* Corresponding author phone: +81-29-8475864; e-mail: y-kawakami@hhc.eisai.co.jp.

<sup>†</sup> Eisai Tsukuba Research Laboratories.

<sup>‡</sup> Eisai Research Institute of Boston.

**Table 1.** Inhibitory Activity of f152A1 and Its Analogues<sup>a</sup>

Name	Structure	TNF-PLAP (nM)	Actin-PLAP (nM)
1 f152A1 (LL-Z-1640-2) (5Z-7-oxo-zeaenol)		11 ± 1	2,372 ± 108
2 f152D2 (Hypothemycin)		36 ± 3	3,580 ± 320
3 f152B1		349 ± 61	3,120 ± 818
4 f152C		>10,000	>10,000

<sup>a</sup> TNF-PLAP (TNF $\alpha$ -PLAP reporter cells, THP-1-33 cells<sup>10</sup>): A TNF $\alpha$ -PLAP plasmid (TNF $\alpha$ -promoter + 5'-UTR (1.4 kb) + PLAP + SV40 polyA + PGK-neo<sup>11</sup>) was constructed with a slight modification in which TNF $\alpha$ -3'-UTR (772 bp) was inserted between PLAP and SV40 polyA (TNF $\alpha$ -promoter + 5'-UTR (1.4 kb) + PLAP + TNF $\alpha$ -3'-UTR + SV40 polyA + PGKneo). Next, the TNF $\alpha$ -PLAP reporter cells were established by stably transfecting the modified TNF $\alpha$ -PLAP plasmid into THP-1 cells. Actin-PLAP ( $\beta$ -actin-PLAP reporter cells, B164 cells<sup>10</sup>): To evaluate non-specific effects of test compounds on transcription in parallel,  $\beta$ -actin-PLAP reporter cells were also established by stably transfecting  $\beta$ -actin-PLAP plasmid ( $\beta$ -actin-promoter (4.3 kb) + PLAP + SV40 polyA + PGKneo) into THP-1 cells. Cell-based assays with TNF $\alpha$ -PLAP and  $\beta$ -actin-PLAP reporter cells: Cells were maintained in RPMI1640 containing 10% heat-inactivated endotoxin-free fetal bovine serum (FBS) and G418 (1 mg/mL). These cells were seeded at a density of  $1.0 \times 10^4$  cells/well onto 96-well plate, then were cultured in the presence or absence of test compounds for 30 min, followed by stimulation with 100 ng/mL of lipopolysaccharide (LPS; *E. coli* 0127:B08 or 011:B4). Total volume of the reaction mixture was 200  $\mu$ L. After cultivation for 24–48 h, culture supernatant was harvested, and alkaline phosphatase activity in the supernatant was measured.

## RESULTS AND DISCUSSION

**1. Conformational Analysis of f152A1 (1).** To obtain all possible conformations of the flexible 14-membered resorcylic acid lactone f152A1 (**1**), we searched the low energy conformations of **1** by HTMD simulations using the AMBER<sup>14</sup> program. All snapshot structures in the stored frame were subjected to energy minimization calculation continuously by molecular mechanics calculation with MMFF (Merck Molecular Force Field).<sup>15</sup> The snapshot structures were subsequently classified into various types of ring conformations one by one according to the set of 14 torsion angles of the 14-membered ring. Structures containing differences in every corresponding torsion angle within a tolerance value of 30° were classified into the same ring

conformation class. From among these classifications, we selected the 25 lowest energy conformations in the energy range of 10.0 kcal/mol from the lowest one. Next, they were subjected to energy minimization by molecular orbital calculation using MOPAC AM1 PRECISE optimization.

Among the low energy conformers listed in Table 2 and their conformations presented in Figure 2, two conformations, M1(8) and M1(9), surfaced with the highest scores. The lowest energy conformation M1(8) was obtained from both molecular mechanics and molecular orbital methods. The M1(8) conformer has the  $\alpha,\beta$ -unsaturated enone plane perpendicular to the macrocyclic ring. The M1(9) conformer is the second most stable conformer. However, with a score nearly equal to that of M1(8), it was possible that M1(9) corresponds to an active conformation of **1**. One difference between M1(8) and M1(9) is the hydrogen bonding between the ketone at C7 and the hydroxyl groups at C8 and C9. M1(8) has a hydrogen bond between 8-OH and 7-C=O, and “M1(9)” has a hydrogen bond between 9-OH and 7-C=O (Figure 3).

Torsion angles of M1(8) were similar to those of M1(9) except for torsion angles 8, 9, and 10, suggesting that the molecular shape of M1(8) is similar to that of M1(9), except in the C8 and C9 region (Figure 4). The C-3 methyl and *cis*-enone moieties are perpendicular to the phenyl ring, and the double bond of the enone presents less steric hindrance for nucleophilic attack from the side.

M2(8) and M3(8) have very different torsion angles as compared to the M1 conformations. The position and direction of the C-3 methyl group is noticeably different from that of the M1 conformation. Also, the *cis*-enone moiety tilts toward the resorcylic acid lactone ring plane.

**2. Consideration of Addition Reaction as a Mechanism of Inhibition.** The biological assay data in Table 1 also indicate the *cis*-enone moiety has a strong influence on inhibitory activity. As noted above, the X-ray crystal structure of the ERK2/FR148083 complex is consistent with contributions from both the *cis*-enone moiety and the conformation of the 14-membered resorcylic acid lactone ring to inhibitory activity. The X-ray crystal study revealed that the compound binds to the ATP binding site of ERK2, involving a covalent bond to S $\gamma$  of ERK2 Cys166. Formation of a covalent bond in the ERK2/f152A1 complex assures that the inhibitor has high activity for ERK2. Other kinases of the MAPKK family that contain a cysteine residue corresponding to Cys166 of ERK2 may be similarly susceptible to covalent modification. If so, covalent binding to the common cysteine residue in the ATP-binding site is likely to play an important role in the inhibitory activity for these MAP kinases. Sequence alignment of *human* MEK1 and *human* ERK2 reveals that MEK1 has a cysteine residue in the ATP binding site corresponding to S $\gamma$  of ERK2 Cys166, which is covalently bound to the  $\beta$ -carbon in the  $\alpha,\beta$ -unsaturated ketone moiety (Figure 5).

If we postulate a Michael addition reaction at the  $\alpha,\beta$ -unsaturated ketone moiety of these compounds as the possible mechanism of inhibition (Figure 6), reactivity of the enone moiety would likely influence the inhibitory activity of the compounds as we observed (Table 1). The Michael addition commences with nucleophilic attack by a Michael donor such as the  $-S^-$  of a cysteine residue, so we focused on the calculated energy of unoccupied-MOs. Hypothemycin covalently binds to the Cys166 at the ATP-

**Table 2.** Heat of Formation Energies and Torsion Angles in the 14-Membered Ring of Low Energy Conformations of **1**

Torsion No	Atom No.1	Atom No.2	Atom No.3	Atom No.4
1	16	16a	1	17
2	16a	1	2	3
3	1	2	3	4
4	2	3	4	5
5	3	4	5	6
6	4	5	6	7
7	5	6	7	8
8	6	7	8	9
9	7	8	9	10
10	8	9	10	11
11	9	10	11	12
12	10	11	12	12a
13	11	12	12a	16a
14	12	12a	16a	1

## Torsion angles

MD fraction NO.	Class	Mopac6 AM1 1SCF Heat of Formation (kcal/mol)	Mopac6 AM1 Precise Heat of Formation (kcal/mol)
496	m1(8)	-230.98	-254.122
314	m1(9)	-239.345	-254.002
408	m2(8)	-237.148	-251.547
532	m3(8)	-233.482	-250.529
275		-233.54	-250.304
198		-229.777	-249.91
389		-234.772	-249.887
424		-233.4	-249.837
195		-233.168	-249.539
1724		-234.157	-249.363
1535		-234.513	-249.128
434		-231.269	-248.991
11		-231.886	-248.979
550		-230.831	-248.861
528		-231.244	-248.836
99		-230.866	-248.537
201		-231.422	-247.992
1523		-230.671	-247.009
1515		-230.425	-246.785
499		-229.492	-246.631
1540		-229.427	-246.069
1615		-229.589	-245.78
188		-230.174	-240.268
1593		-231.841	-230.847
288		-236.878	-221.998

25 lowest energy conformations in the energy range of 10.0 kcal/mol obtained from HTMD simulations.

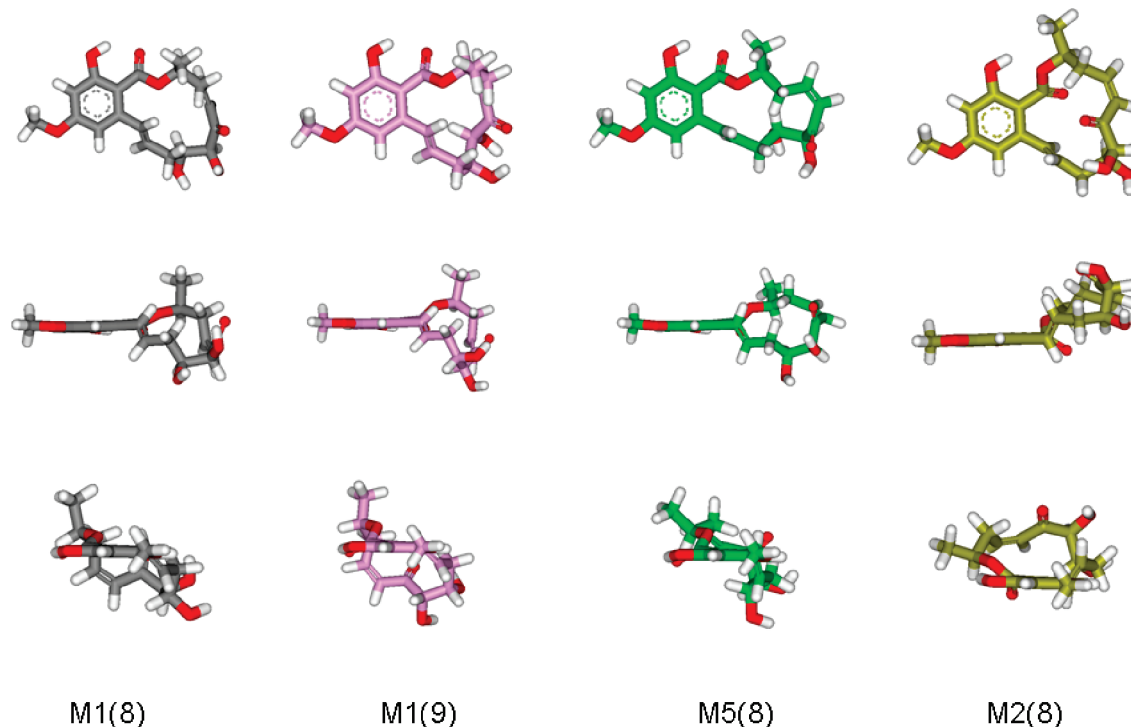
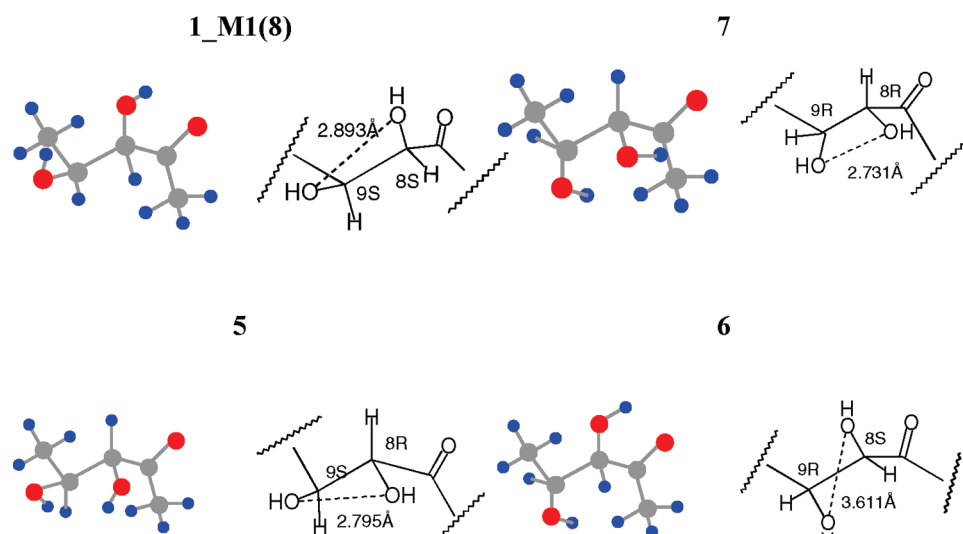
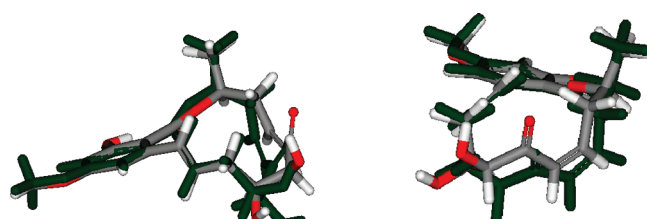
MD fraction No.	Class	Torsion Angle (degree)													
		1	2	3	4	5	6	7	8	9	10	11	12	13	14
496	m1(8)	-22.82	-174.37	-139.68	78.62	-144.02	2.35	145.42	-65.84	-62.56	144.29	-122.4	179	-125.36	-2.15
314	m1(9)	-41.62	-179.33	-98.18	74.33	-133.51	2.34	137.07	-153.66	56.31	59.54	-127.32	179.53	-131.72	-4.57
408	m2(8)	-40.69	175.13	-152.64	148.78	-130.68	0.64	111.24	-86.07	-67.05	161.06	-118.01	176.58	-91.72	-3.32
532	m3(8)	-136.42	172.68	-87.97	112.96	-128.58	1.59	161.82	-69.51	-92.62	73.8	86.54	173.39	107.18	-3.39

## List of torsion angles of 4 lowest energy conformations.

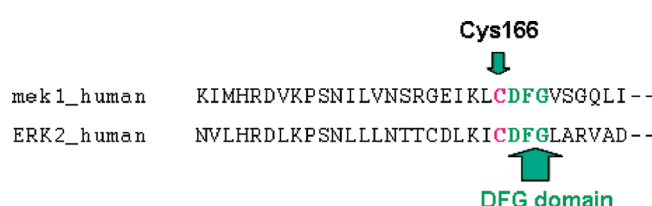
binding site of ERK2 in the M1(8) active conformation. Reactivity of the *cis*-enone moiety and the M1(8) conformation play an important role in the inhibitory activity for these MAP kinases. The  $-S^-$  of Cys166 likely attacks the *cis*-enone from the side at the M1(8) conformation.

**3. Conformational Analysis of f152A1 Diastereomers at the 8,9-Diol Moiety Reveals Effects of the Orientation of the Hydroxyl Groups.** Data from inhibition assay experiments also pointed to the importance of the diol group, and the chirality of the diol group influenced inhibitory activity (Table 3). Changing the stereochemistry of either

or both hydroxyl groups resulted in a 57–65-fold loss of activity. Thus, the effect of the diol moiety on the conformation of the 14-membered benzoxacyclotetradecin ring from conformational analyses of f152A1 diastereomers at the 8,9-diol position was also studied (Table 4). The lowest energy conformation was superimposed on that of f152A1, as shown in Figures 7–9. Only **5** (8*R*, 9*S*), which is the second lowest energy diastereomer of f152A1, can assume the M1(9) conformation (Figure 7); the other two diastereomeric compounds do not form either the M1(8) or the M1(9) conformation. Interestingly, the lowest energy conformation

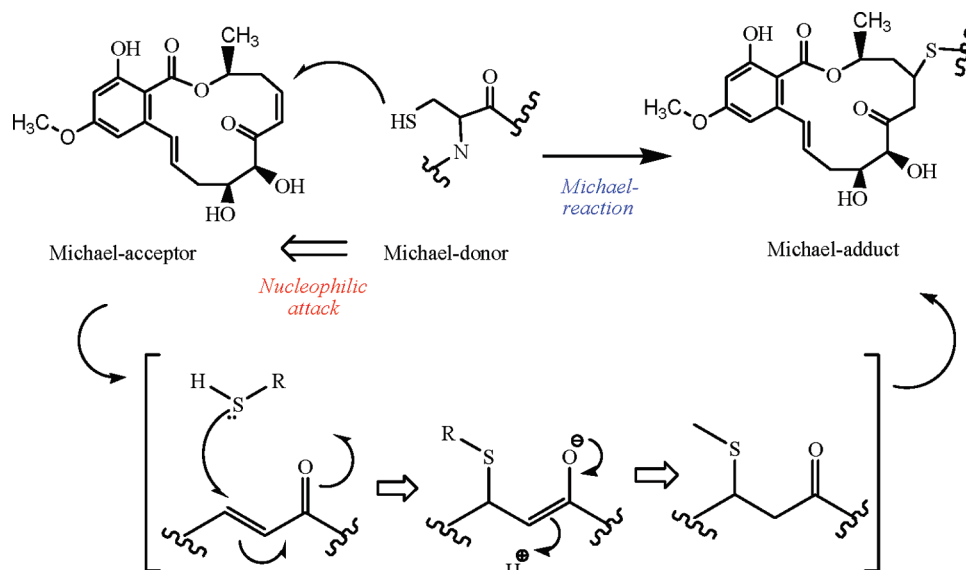
**Figure 2.** Stable conformations of **1**.**Figure 3.** Lowest energy stable conformations of the C8,C9-diol moiety.**Figure 4.** Superimposition of **1\_M1(8)** and **1\_M1(9)**. **1\_M1(8)** conformation is presented in default color, and **1\_M1(9)** is in red.

of **7** (*8R, 9R*) was just like the mirror image of **1\_M1(8)** conformation (Figure 9b), and no M1 conformations were found in the energy range of 10.0 kcal/mol from the lowest one. It can be concluded that the low energy conformations of these diastereomers are different from that of **1**, and that the M1 conformation may contribute to the activity of

**Figure 5.** Sequence alignment of *human MEK1* and *human ERK2*. The position of Cys166 is indicated by a green arrow, and the DFG domain is also.

f152A1. According to the conformation analysis results, the ring conformations of f152A1 diastereomers at the 8,9-diol were different, and considering that compounds **5** and **6** have reduced activity as compared to **1**, the orientation of the OH groups also contributes to inhibitory activity.

The unoccupied MOs at the enone moiety are underlined in Table 5. The (L+1)UMO orbital of f152A1 extends over

**Figure 6.** Michael reaction mechanism for f152A1.**Table 3.** TNF- $\alpha$  PLAP Transcription Assay Data for Diastereomers at the C8,C9-Diol Moiety<sup>a</sup>

Compound	<b>1</b> (8S, 9S)	<b>5</b> (8R, 9S)	<b>6</b> (8S, 9R)	<b>7</b> (8R, 9R)
Structure				
Activity * (nM)	11	691	622	711

<sup>a</sup> The “\*” represents the Inhibitory effect on TNF- $\alpha$  PLAP transcription. For general information on assays, please see footnote of Table 1.

the enone moiety (Figure 10). Relative reactivity was determined by comparing the underlined eigenvalue to that of the **1**\_M1(8) conformation, and this index value became a measure of reactivity. A negative value is indicative that the compound has a Michael addition reactivity higher than 1.

Compounds **5**, **6**, and **7**, diastereomers of f152A1, have activities 57–65-fold weaker than f152A1. These can be rationalized as follows.

The molecular shape of the M1(9) conformation is similar to that of M1(8), but possesses reduced reactivity for the

Michael addition reaction. M1(9) is probably not the active conformation of f152A1.

Compound **5** has lower Michael reactivity.

Compounds **6** and **7** do not appear to adopt the active M1(8) or M1(9) conformations.

**4. Estimating the Effects of Alterations at the C3 Position of f152A1.** Inhibitory potency as assessed in the TNF $\alpha$  PLAP reporter assay was also reduced by either removal of (10-fold reduction) or alteration of the stereochemistry (over 150-fold reduction) of the methyl group at

**Table 4.** Lowest Energy Conformations of f152A1 and Its Diol Diastereomers

	conformation	HOF <sup>a</sup> /kcal/mol	relative energy kcal/mol	rmsd <sup>b</sup>
<b>1</b> (f152A1)	lowest	M1(8)	-254.12	0.00
	second lowest	M1(9)	-254.00	+0.12
<b>5</b>	lowest	M1(9)	-253.36	0.00
	second lowest	M1(8)	-251.92	+1.44
<b>6</b>	lowest			>+10.00
	second lowest	M1(9)	-252.83	0.00
<b>7</b>	lowest	M1(8)	-252.29	+0.52
	second lowest	M1(9)	-251.21	+1.61
			-248.68	+4.15
			-253.40	0.00
			-253.22	+0.18
				2.41 Å
				1.78 Å

<sup>a</sup> HOF: Heat of formation. <sup>b</sup> rmsd: Root-mean-square deviation of 14-membered ring atoms between each lowest energy conformation and that of **1**.

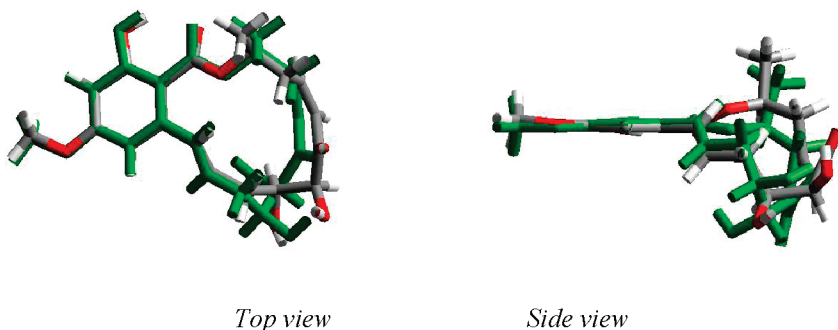


**Figure 7.** Superimposition of f152A1 (**1**) and its diol diastereomer **5**. f152A1 (**1**) is presented by stick model in default color, and **5** is in green.

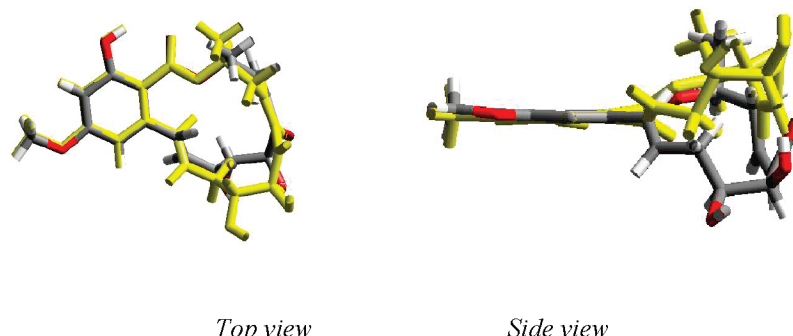


**Figure 8.** Superimposition of f152A1 (**1**) and its diol stereoisomer **6**. f152A1 (**1**) is presented by stick model in default color, and **6** is in yellow.

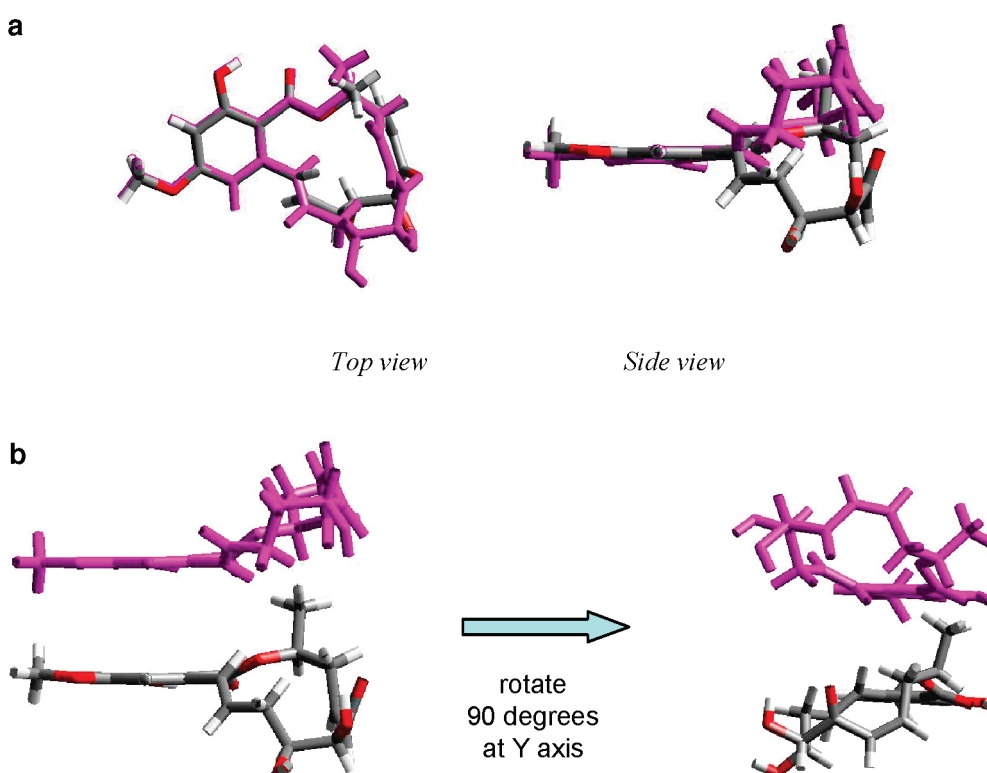


**Figure 9.** (a) Superimposition of f152A1 (**1**) and its diol diastereomer **7**. f152A1 (**1**) is presented by stick model in default color, and **7** is in magenta. (b) Mirror image-like conformations of f152A1 (**1**) and **7**, viewing from the enone plane. f152A1 (**1**) is presented by stick model in default color, and **7** is in magenta.

the C3 position (Table 6). HTMD conformation searches of **1** and two C3 modified compounds were carried out (Table 7).

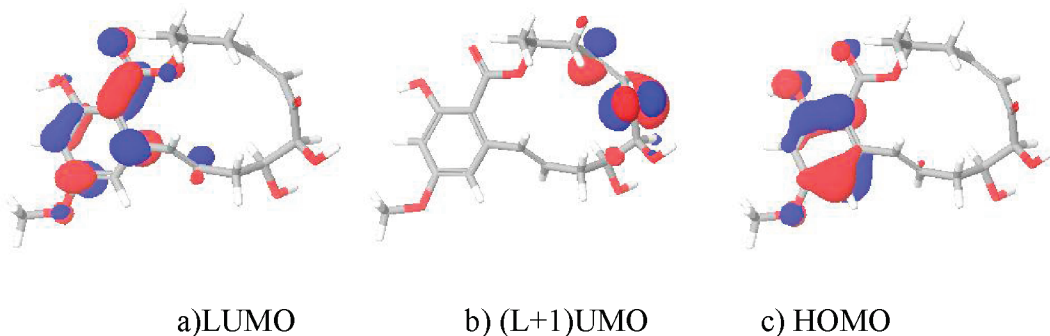
It was found that **8** has M1(8) as the lowest energy conformer (Figure 11), while **9** showed as a mix of M1(8) and M1(9) conformations (Figure 12). It was concluded that compounds **8** and **9** can exist in the same conformation as

**1**, M1(8) or M1(9). These results suggest that there exists a hydrophobic pocket around the C3 position when these compounds interact with the enzyme binding site: The 3S-methyl group fits in the pocket, but the 3R-methyl group apparently disturbs the interaction and displays a reduction in activity of over 150-fold.

**Table 5.** Reactivity of the Enone Moiety in f152A1 and Its Diol Diastereomers<sup>a</sup>

Compound	Structure	Conformation	HOF (kcal/mol)	*1 Eigenvalue (eV)	*2 Relative Reactivity	*3 Activity (nM)
<b>1</b> <b>f152A1</b> <i>8S,9S</i>		M1(8)	-254.12	<u>-0.32410</u>	0.0	11
		M1(9)	-254.00	<u>-0.09415</u>	0.22995	
<b>5</b> <i>8R,9S</i>		M1(9)	-253.36	<u>-0.10923</u>	0.21487	691
<b>6</b> <i>8S,9R</i>		other	-252.83	<u>-0.34927</u>	-0.02517	622
<b>7</b> <i>8R,9R</i>		other	-253.40	<u>-0.31219</u>	0.01191	711

<sup>a</sup> “\*1”: (L+1) UMO orbital eigenvalue extending over enone moiety. “\*2”: Relative reactivity for Michael reaction as compared to the enone moiety of **1**\_M1(8). Eigenvalue difference from enone moiety of **1**\_M1(8). “\*3”: Inhibitory effect on TNF- $\alpha$  PLAP transcription. For general information on assays, please see footnote of Table 1.

**Figure 10.** Molecular orbital of **1**\_M1(8) conformation.**Table 6.** TNF- $\alpha$  PLAP Transcription Assay Data for f152A1 Derivatives at C3 Substituents<sup>a</sup>

<b>f152A1 , 1 (3<i>S</i>)</b>	<b>8 (3<i>R</i>)</b>	<b>9 (des 3-Me)</b>
Activity*: 11.0 nM	1,048 nM	69.0 nM

<sup>a</sup> The “\*” represents inhibitory effect on TNF- $\alpha$  PLAP transcription. For general information on assays, please see footnote of Table 1.

Enone reactivity results with C3 analogues are summarized in Table 8. Relative reactivity was determined by comparing the underlined eigenvalue to that of the **1**\_M1(8) conformation, and this index value became a measure of reactivity. A negative value is indicative that the compound has a Michael addition reactivity higher than **1**. Based on this analysis, the

calculated enone reactivity of **8** is nearly equal to that of **1**, while that of **9** is only reduced in the M1(9) conformation. It seems that the reduced inhibitory activity of **9** can be attributed to decreased reactivity of the enone. The difference between **8** and **9** in relative reactivity and potency suggests that an additional factor, configuration of the C3-methyl,

**Table 7.** HTMD Conditions and Stable Conformations

	<b>8</b> (3 <i>R</i> )	<b>9</b> (des 3-Me)
HTMD temperature	1500 K	2500 K
simulation period	100 ps	100 ps
total no. of frames	2000	2000
no. of <i>cis</i> -enone frames	2000	1157
lowest energy (kcal/mol)	-253.52	-250.67
conformation	M1(8)	M1(9)
rmsd with f152 M1(8)	0.28 Å	
second lowest	-253.09	-250.58
conformation	M1(9)	M1(8)
rmsd with f152 M1(8)		0.22 Å

which can influence the steric interaction of a compound with the target protein, is in play. It also suggests that the hydrophobic pocket for C3-methyl is at the binding site of the enzyme, favoring the (*S*) configuration.

**5. Importance of the *cis*-Enone Moiety.** The trans form of f152A1, **3**, possesses reactivity nearly equal to that of **1** (Table 9). Although the enone of **3** is still perpendicular to the macrocyclic ring as in **1**, **3** has a different orientation of 8,9-diol moieties as compared to **1** (Figure 13). These results suggest that the 32-fold reduction in inhibitory activity of **3** may be due to a conformational difference relative to the M1(8) conformation.

## CONCLUSION

The conformation analysis of the 14-membered macrocyclic ring, and molecular orbital studies of the *cis*-enone moiety of f152A1 and its analogues, were correlated with SAR data. The results suggest that: (i) the enone is a Michael acceptor reactive with enzyme; (ii) the active conformation is M1(8), in which an intermolecular hydrogen bond between 8-OH and the enone oxygen increases reactivity of the enone moiety; and (iii) the 8,9-diol restrains the 14-membered ring conformation.

These findings further suggest that the structural features of f152A1 that contribute to its kinase inhibition activity as assessed by the TNF $\alpha$  PLAP reporter assay are as follows:

(1) The *cis*-enone group participates in a Michael reaction and conformationally restrains f152A1.

(2) The 3*S*-methyl group fills a small pocket at the active site of ERK2 and MEK1. The 3*R*-methyl group contacts the main chain and destabilizes the interaction energy, which resulted in reduced potency (100-fold).

(3) The *cis*-enone moiety likely faces toward the cysteine residue at the active site.

(4) The 8,9-diol constrains the conformation of f152A1.

The presence of a cysteine residue in the active site of each of ERK2 and MEK1 is consistent with the postulated Michael addition reaction, and our finding that higher reactivity of the enone, among other features, correlates with higher potency of inhibition *in vitro*. Although f152A1 can inhibit MEKK1 kinase activity,<sup>16</sup> the absence of a corresponding cysteine residue at the active site suggests that additional studies of f152A1 and its analogues are needed to understand the mechanism of inhibition of MEKK1.

## EXPERIMENTAL SECTION

**Molecular Dynamics Simulations.** All of the MD calculations were performed using the AMBER program (version 3.0, revision A). For the energy minimization of the stored snapshot structures from the trajectory, a program in AMBER was modified, so as to perform calculations continuously.

Three-dimensional models were prepared on the basis of the crystal structure of "Radicicol". All hydrogen atoms in the molecules were relocated at the geometrically expected positions. The structures were optimized by the MNDO method in the MOPAC program.

The formal atomic charges used for the MD and subsequent molecular mechanics calculations were obtained from those of the optimized structures.

The starting structures were energy-minimized using the same force field parameters as for the MD calculations.

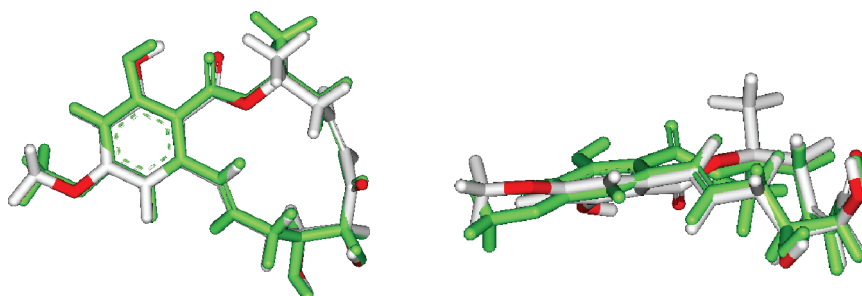


**Figure 11.** Superimposition of **1**\_M1(8) and **8**\_M1(8) conformations. f152A1 (**1**) is presented by stick model in default color, and **8** is in green.

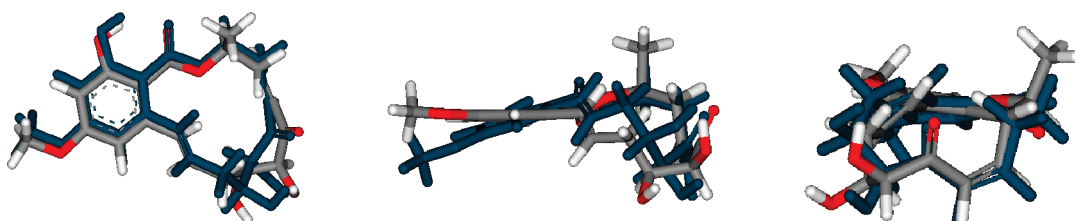


**Figure 12.** Superimposition of **1**\_M1(8) and **9**\_M1(9) conformations. f152A1 (**1**) is presented by stick model in default color, and **9** is in blue.

**Table 8.** Reactivity of the Enone Moiety in f152A1 and C3 Analogues<sup>a</sup>

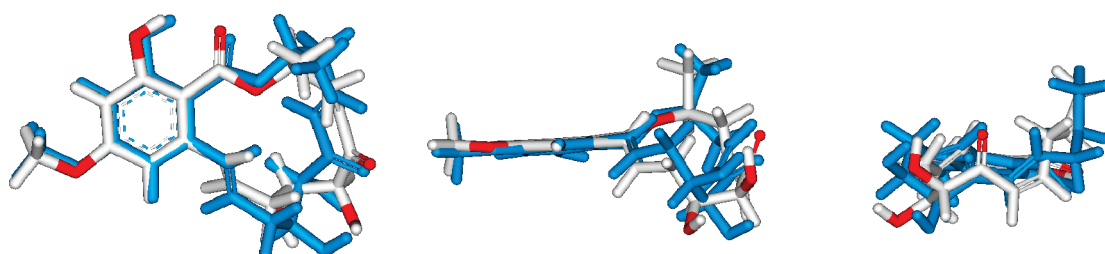
Compound	Structure	Conformation	HOF (kcal/mol)	*1 Eigenvalue (eV)	*2 Relative Reactivity	*3 Activity (nM)
<b>1</b> f152A1 3S		M1(8)	-254.12	<u>-0.32410</u>	0.0	11
<b>8</b> 3R		M1(8)	-253.52	<u>-0.32502</u>	-0.00092	1,048
<b>9</b> des 3-Me		M1(9)	-250.67	<u>-0.08684</u>	0.23726	69
		M1(8)	-250.58	<u>-0.30135</u>	0.02275	69

<sup>a</sup> “\*1”: (L+1) UMO orbital eigenvalue extending over enone moiety. “\*2”: Relative reactivity for Michael reaction as compared to the enone moiety of **1**\_M1(8). Eigenvalue difference from enone moiety of **1**\_M1(8). “\*3”: Inhibitory effect on TNF- $\alpha$  PLAP transcription. For general information on assays, please see footnote of Table 1.

**Table 9.** Reactivity of the Enone Moiety in f152A1 and Trans Form Compound **3**<sup>a</sup>

Compound	Structure	Conformation	HOF (kcal/mol)	*1 Eigenvalue (eV)	*2 Relative Reactivity	*3 Activity (nM)
<b>1</b> f152A1		M1(8)	-254.12	<u>-0.32410</u>	0.0	11
<b>3</b> f152B1		other	-252.10	<u>-0.32822</u>	-0.00412	349

<sup>a</sup> “\*1”: (L+1) UMO orbital eigenvalue extending over enone moiety. “\*2”: Relative reactivity for Michael reaction as compared to the enone moiety of **1**\_M1(8). Eigenvalue difference from enone moiety of **1**\_M1(8). “\*3”: Inhibitory effect on TNF- $\alpha$  PLAP transcription. For general information on assays, please see footnote of Table 1.

**Figure 13.** Superimposition of compound **1**\_M1(8) and **3**. f152A1 (**1**) is presented by a stick model in default color, and **3** is in blue.

Molecular dynamics calculations were subsequently performed for equilibration at 300 K for 10 ps. The high-temperature MD calculations were carried out at 3000 K. The simulations lasted for 100 ps with the time step of 1.0 fs. Solvent molecules were not included in the calculations. The frame data were stored every 50 steps, giving 2000 frames after a 100 ps simulation. The dielectric constant value is 4.0.

At the beginning of a classification, the template list of referential conformations contained the first frame structure only. Structures whose difference in every corresponding torsion angle was within a tolerance value of 30° were classified into the same ring conformation. If some of the differences were outside the given tolerance values, the structure was added to the template structure list as a new referential conformation. All snapshot structures in the stored frame were subjected to energy minimization calculation continuously by MMFF (Merck Molecular Force Field). Next, the snapshot structures were classified into typical ring conformations one by one according to the set of 14 torsion angles of the 14-membered ring.

After the classification, we selected the lowest 20 energy structures in the stored frame, and they were subjected to energy minimization by MOPAC AM1 PRECISE optimization.

The program package, Discover Studio ver.2.1,<sup>17</sup> was used in superimposition and molecular modeling.

#### ACKNOWLEDGMENT

We are grateful to Drs. Tomohiro Matsushima, Hiroshi Shirota, Fabian Gusovsky, and Mr. Kenichi Chiba for their valuable suggestions. We also thank Drs. Lucian DiPietro, Sandra Gilbert, Jean-Christopher Harmange, Masanori Fujita, and Satoshi Yamamoto for providing chemical and biological information.

#### REFERENCES AND NOTES

- (1) Ellestad, G. A.; Lovell, F. M.; Perkinson, N. A.; Hargreaves, R. T.; McGahren, W. J. New zearalenone related macrolides and isocoumarins from an unidentified fungus. *J. Org. Chem.* **1978**, *43*, 2339–2343.
- (2) Rawlins, P.; Mander, T.; Sadeghi, R.; Hill, S.; Gammon, G.; Foxwell, B.; Wrigley, S.; Moore, M. Inhibition of endotoxin-induced TNF- $\alpha$  production in macrophages by 5Z-7-oxo-zeaenol and other fungal resorcylic acid lactones. *Int. J. Immunopharmacol.* **1996**, *17*, 887–894.
- (3) Ohori, M.; Kinoshita, T.; Yoshimura, S.; Warizaya, M.; Nakajima, H.; Miyake, H. Role of a cystein residue in the active site of ERK and the MAPKK family. *Biochem. Biophys. Res. Commun.* **2007**, *353*, 633–637.
- (4) Shaulian, E.; Karin, M. AP-1 as a regulator of cell life and death. *Nat. Cell Biol.* **2002**, *4*, E131–E136.
- (5) Young, M. R.; Yang, H. S.; Colburn, N. H. AP-1 consists of 18 dimeric combinations of the families Jun (c-Jun, JunB and JunD) and Fos (c-Fos, FosB, Fra-1 and Fra-2). *Trends Mol. Med.* **2003**, *9*, 36–41.
- (6) Agatsuma, T.; Takahashi, A.; Kubuto, C.; Nozoe, S. Revised structure of hypothemycin. *Chem. Pharm. Bull.* **1993**, *41*, 373–375.
- (7) Schirmer, A.; Kennedy, J.; Murli, S.; Reid, R.; Santi, D. V. Targeted covalent inactivation of protein kinases by resorcylic acid lactone polyketides. *Proc. Natl. Acad. Sci. U.S.A.* **2006**, *103*, 4234–4239.
- (8) Nair, M. S. R.; Carey, S. T.; James, J. C. Metabolites of pyrenomycetes. XIV: Structure and partial stereochemistry of the antibiotic macrolides hypothemycin and dihydrohypothemycin. *Tetrahedron* **1981**, *37*, 2445–2449.
- (9) Rastelli, G.; Rosenfeld, R.; Reid, R.; Santi, D. V. Molecular modeling and crystal structure of ERK2-hypothemycin complexes. *J. Struct. Biol.* **2008**, *164*, 18–23.
- (10) Goto, M.; Yamada, K.; Katayama, K.; Tanaka, I. Inhibitory effect of E3330, a novel quinone derivative able to suppress tumor necrosis factor-alpha generation, on activation of nuclear factor-kappa B. *Mol. Pharmacol.* **1996**, *49*, 860–873.
- (11) Goto, M.; Chow, J.; Muramoto, K.; Chiba, K.; Yamamoto, S.; Fujita, M.; Obaishi, H.; Tai, K.; Mizui, Y.; Tanaka, I.; Young, D.; Yang, H.; Wang, Y. J.; Shirota, H.; Gusovsky, F. E6201 [(3S,4R,5Z,8S,9S,11E)-14-(Ethylamino)-8, 9,16-trihydroxy-3, 4-dimethyl-3,4,9,19-tetrahydro-1H-2-benzoxacyclotetradecine-1,7(8H)-dione], a novel kinase inhibitor of mitogen-activated protein kinase/extracellular signal-regulated kinase (MEK)-1 and MEK kinase-1: In vitro characterization of its anti-Inflammatory and antihyperproliferative activities. *J. Pharmacol. Exp. Ther.* **2009**, *331*, 485–495.
- (12) Kawai, T.; Ichinose, T.; Endo, Y.; Shudo, K.; Itai, A. Active conformation of a tumor promoter, teleocidin. A molecular dynamics study. *J. Med. Chem.* **1992**, *35*, 2248–2253.
- (13) Stewart, J. J. P. MOPAC A semiempirical molecular orbital program. *J. Comput.-Aided Mol. Des.* **1990**, *4*, 1–105.
- (14) Weiner, S. J.; Kollman, P. A.; Case, D.; Singh, U. C.; Ghio, C.; Alagona, G.; Profeta, S.; Weiner, P. K. A new force field for molecular mechanical simulation of nucleic acids and proteins. *J. Am. Chem. Soc.* **1984**, *106*, 765–784.
- (15) Halgren, T. A. Merck Molecular Force Field. V. Extension of MMFF94 using experimental data, additional computational data and empirical rules. *J. Comput. Chem.* **1996**, *17*, 616–641.
- (16) Data are not shown.
- (17) *Discover Studio, version 2.1*; Accelrys Software Inc.: San Diego, CA, 2008.

CI9003128